PHYSICAL REVIEW B **94**, 184511 (2016)

Direct observation of charge order in underdoped and optimally doped $Bi_2(Sr,La)_2CuO_{6+\delta}$ by resonant inelastic x-ray scattering

Y. Y. Peng,[1,*] M. Salluzzo,[2] X. Sun,[3] A. Ponti,[4] D. Betto,[5] A. M. Ferretti,[4] F. Fumagalli,[6] K. Kummer,[5] M. Le Tacon,[7,8] X. J. Zhou,[3] N. B. Brookes,[5] L. Braicovich,[1] and G. Ghiringhelli[1,9,†]

[1]*Dipartimento di Fisica, Politecnico di Milano, Piazza Leonardo da Vinci 32, I-20133 Milano, Italy*

[2]*CNR-SPIN, Complesso Monte Sant'angelo, Via Cinthia, I-80126 Napoli, Italy*

[3]*Beijing National Laboratory for Condensed Matter Physics, Institute of Physics, Chinese Academy of Sciences, 100190 Beijing, China*

[4]*Istituto di Scienze e Tecnologie Molecolari, Via Camillo Golgi 19, I-20133 Milano, Italy*

[5]*ESRF, The European Synchrotron, CS 40220, F-38043 Grenoble Cedex, France*

[6]*Italian Institute of Technology-Center for Nanoscience and Technology, Via Pascoli 70/3, 20133 Milano, Italy*

[7]*Max-Planck-Institut für Festkörperforschung, Heisenbergstraße 1, D-70569 Stuttgart, Germany*

[8]*Karlsruher Institut für Technologie Institut für Festkörperphysik Hermann-v.-Helmholtz-Platz 1, D-76344 Eggenstein-Leopoldshafen, Germany*

[9]*CNR-SPIN and CNISM, Politecnico di Milano, Piazza Leonardo da Vinci 32, I-20133 Milano, Italy*

(Received 5 October 2016; revised manuscript received 7 November 2016; published 28 November 2016)

Charge order in underdoped and optimally doped high-T_c superconductors $Bi_2Sr_{2-x}La_xCuO_{6+\delta}$ (Bi2201) is investigated by Cu L_3 edge resonant inelastic x-ray scattering. We have directly observed charge density modulation in the optimally doped Bi2201 at momentum transfer $Q_\parallel \simeq 0.23$ reciprocal lattice units, with smaller intensity and correlation length with respect to the underdoped sample. This demonstrates the short-range charge order in Bi2201 persists up to optimal doping, as in other hole-doped cuprates. We explored the nodal (diagonal) direction and found no charge order peak, confirming that charge density modulates only along the Cu-O bond directions. We measured the out-of-plane dependence of charge order, finding a flat response and no maxima at half integer L values. This suggests there is no out-of-plane phase correlation in single layer Bi2201, at variance from $YBa_2Cu_3O_{6+x}$ and $La_{2-x}(Ba,Sr)_xCuO_4$. Combining our results with data from the literature we assess that charge order in Bi2201 exists in a large doping range across the phase diagram, i.e., $0.07 \lesssim p \lesssim 0.16$, demonstrating thereby that it is intimately entangled with the antiferromagnetic background, the pseudogap, and superconductivity.

DOI: 10.1103/PhysRevB.94.184511

I. INTRODUCTION

The search for the underlying mechanism of high-T_c superconductivity in cuprates is still active after 3 decades since its discovery [1]. The insulating parent compounds become superconductors by chemical doping, which modifies the charge balance of the CuO_2 planes and rapidly suppresses their two-dimensional (2D) long-range antiferromagnetic order [2]. In the "normal" state, above the superconducting critical temperature T_c, there is an exotic pseudogap phase whose origin and relation to the superconducting phase are still much debated [3]. More recently, evidence of charge order, or the charge density wave (CDW), within the CuO_2 planes has been found, below optimal doping, in several families [4–20], further increasing the complexity of the cuprates' phase diagram [21]. The temperature evolution of the CDW [10] and its behavior under magnetic fields [12,22,23] have indicated that charge order is in competition with superconductivity. Although the phenomenology of the CDW has grown fast, it is still patchy and a systematic knowledge of its doping evolution would help clarify its role in high-T_c superconductivity and its relation with the quantum critical points (QCP) in the phase diagram.

Early evidence of bulk charge order was obtained in La-based cuprates by inelastic neutron scattering (INS) near the hole doping $p = 1/8$ [4,5] and later by x-ray scattering with an approximately commensurate wave vector, $Q_\parallel \simeq 0.25$ reciprocal lattice units (rlu) [7]. More recently, an incommensurate charge order at $Q_\parallel \simeq 0.31$ rlu along the Cu-O bond direction has been observed by various techniques in $(Y,Nd)Ba_2Cu_3O_{6+x}$ (YBCO, NBCO) [9–13], which might be responsible for the Fermi surface reconstructions in high magnetic fields giving rise to quantum oscillations [24,25]. Soon after, the enhanced sensitivity of resonant x-ray scattering also allowed the detection of a short-range charge order in $Bi_2Sr_{2-x}La_xCuO_{6+\delta}$ (Bi2201) [14], $Bi_2Sr_2CaCu_2O_{8+\delta}$ (Bi2212) [15,16], and $HgBa_2CuO_{4+\delta}$ [17], and eventually in electron-doped $(Nd,La)_{2-x}Ce_xCuO_4$ [19,20], indicating its ubiquity in cuprate superconductors. Hereafter we confine our discussion to hole-doped systems for brevity. The CDW is strongest in the underdoped regime and persists up to optimal doping [8,16,18]. In Bi2201, the charge order was observed by resonant x-ray scattering (RXS) in the underdoped region ($p \sim 0.115 - 0.145$) with the wave vector, decreasing with p, that was proposed to match the distance between the tips of the ungapped segments of the Fermi surface ("Fermi arcs") [14]. A previous resonant inelastic x-ray scattering (RIXS) study on optimally doped Bi2201 (OP-Bi2201) has not found a charge order signal directly [26]. Instead a low-energy feature at $Q_\parallel \simeq 0.22$ rlu was observed up to 200 K and was attributed to a phonon signal. On the other hand, in OP-Bi2201

*yingying.peng@polimi.it
†giacomo.ghiringhelli@polimi.it

surface-sensitive techniques have revealed a quite different scenario. Angle-resolved photoemission spectroscopy (ARPES) has shown a particle-hole symmetry breaking and a phase transition below the pseudogap temperature [27,28], and scanning tunneling microscopy (STM) has found a checkerboardlike electronic modulation in a broad doping range of Bi2201 [29]. However, electronic states may vary in bulk (studied with x rays) and at the surface (studied with STM and ARPES).

The discrepancy between bulk and surface measurements calls for a more accurate investigation: here, by using high-resolution RIXS at the Cu L_3 edge, we study the charge order in underdoped ($T_c = 15$ K, UD15K) and optimally doped ($T_c = 33$ K, OP33K) $Bi_2Sr_{2-x}La_xCuO_{6+\delta}$. We focus on the quasielastic spectral component that is sensitive to charge modulations [10]. Along the Cu-O bond direction, we observed a bulk charge order peak at incommensurate vector $Q_\parallel \simeq 0.26$ (0.23) rlu in UD15K (OP33K). This expands up to optimal doping the region where charge order, superconductivity, and pseudogap coexist in B2201. We also performed temperature measurements on OP33K across T_c and T^* to investigate the relations between charge order, superconductivity, and pseudogap. We notice that a prior energy-integrated RXS measurement on Bi2201 reported no CDW signatures along the diagonal (nodal) direction [30]. However, the checkerboardlike features observed by STM [29] are compatible with a 2D CDW structure, as opposed to the 1D stripelike shape proposed for YBCO [30]. Here we use energy-resolved RIXS and its higher sensitivity to ascertain this issue. Finally, in UD15K we measured the charge order peak intensity along the c^* direction [we quote (H,K,L) for wave vector coordinates in pseudotetragonal structure] to understand the out-of-plane phase correlation, and we compare the results to the antiphase correlations in $YBa_2Cu_3O_{6+x}$ [31] and $La_{2-x}(Ba,Sr)_xCuO_4$ [6–8].

II. EXPERIMENTAL METHOD

The phase diagram of $Bi_2Sr_{2-x}La_xCuO_{6+\delta}$ [32] is shown in Fig. 1(a). By substitution of Sr by La we can span a wide range of doping. Here we study the underdoped (UD15K, $p \simeq 0.115$) and the optimally doped (OP33K, $p \simeq 0.16$) samples, as indicated by the arrows in the figure. The high-quality single crystals were grown by the floating zone method. The hole concentration was optimized by annealing the samples in O_2 flow and the T_c values were determined from the magnetization measurements as shown in Fig. 1(b), which displayed sharp transition widths ~3 K. The sample growth and characterization methods were reported in Ref. [33]. The RIXS measurements were performed with the ERIXS spectrometer at the beam line ID32 of ESRF (The European Synchrotron, Grenoble, France). The x-ray energy was tuned to the maximum of the Cu L_3 absorption peak around 931 eV. The experimental energy resolution was ~70 meV. The samples were cleaved out-of-vacuum just before installation inside the vacuum measurement chamber, to reduce surface contamination and oxygen depletion.

The experimental geometry is shown in Fig. 1(c). X-rays are incident on the sample surface and scattered by 2θ, which can be changed continuously from 50° to 150°. The x-ray

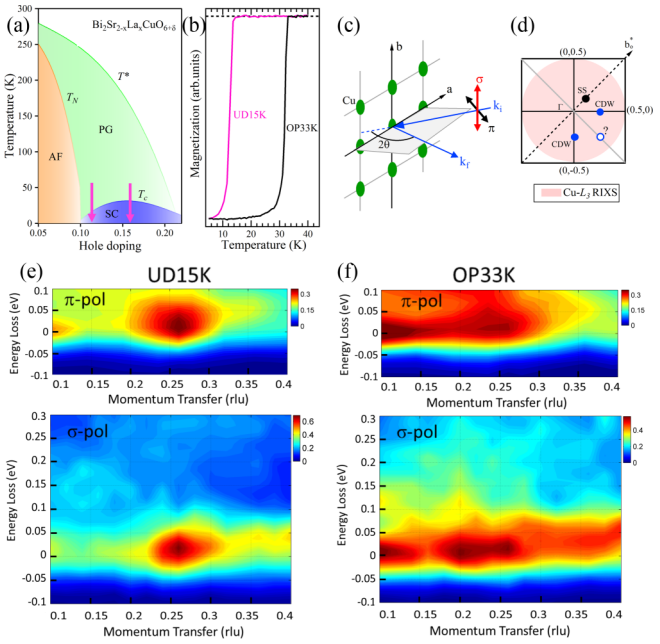

FIG. 1. (a) Schematic temperature-doping phase diagram of $Bi_2(Sr,La)_2CuO_{6+\delta}$. It shows the antiferromagnetic (AF) region defined by T_N, superconducting (SC) region defined by T_c, and the pseudogap (PG) region defined by T^*, which are reproduced from NMR measurements of Ref. [32]. Here we study two doping levels as indicated by the arrows. (b) Magnetization measurements of the Bi2201 single crystals with a magnetic field of 1 Oe. (c) The experimental geometry. The incident photon polarization can be chosen parallel (π) or perpendicular (σ) to the scattering plane. (d) Reciprocal-space image. The accessible reciprocal space in Cu L_3 RIXS experiments with 150° scattering angle is indicated by the pink circle. In Bi-based cuprates there is a well-known superstructure (SS) as indicated by the black circle along the b_o^* direction. (e) Energy/momentum intensity maps of RIXS spectra along the (0,0)-(0.5,0) symmetry direction taken with π- or σ-polarized incident light at 20 K for UD15K. (f) Same as panel (e) but for OP33K.

polarization can be chosen parallel (π) or perpendicular (σ) to the horizontal scattering plane. Reciprocal lattice units (rlu) were defined using the pseudotetragonal unit cell with $a = b = 3.86$ Å and $c = 24.4$ Å, where the axis c is normal to the cleaved sample surface. The sample can be rotated azimuthally around the c axis to choose the in-plane wave-vector component. We determined accurately the orientations of our Bi2201 samples by utilizing the [002] Bragg peak and the superstructure peak. The typical size of the Brillouin zone along the [1,0] direction in cuprates is ~0.81 $Å^{-1}$ and the maximum total momentum transfer at the Cu L_3 edge with $2\theta = 150°$ is ~0.85 $Å^{-1}$, which allows one to cover the whole first magnetic Brillouin zone as indicated by the pink area in Fig. 1(d). The well-known incommensurate supermodulation (superstructure) in the Bi-based cuprates, due to the distortions of the BiO bilayers, projects along the b_o^* direction in the orthorhombic notation [34], giving a peak around $[Q_{ss}, Q_{ss}]$ in pseudotetragonal notation, with $Q_{ss} \simeq 1/8$ rlu. In the same notation charge order is observed along both the (0,0)-(0.5,0) and (0,0)-(0,0.5) directions. Along the diagonal we performed the measurement only along the (0,0)-(0.5,−0.5) direction, to

avoid confusion with the intense superstructure peak and its replicas along the same direction. We present RIXS spectra normalized to the integrated intensity of the *dd* excitations following previous conventions [35]. The zero energy-loss position was determined by measuring, for each transferred momentum, a nonresonant spectrum of silver paint or carbon tape.

III. RESULTS

A. Doping dependence

Figure 1(e) displays the energy/momentum intensity maps of RIXS spectra for UD15K along the (0,0)-(0.5,0) symmetry direction, collected at $T = 20$ K with both π- and σ-polarized incident x rays. Both maps exhibit a charge order signal around the quasielastic energy region, with similar wave vector as reported by RXS [14]. In Fig. 1(f), we have identified a bulk charge order in OP33K with both π- and σ-polarized incident x rays. The charge order signal in OP33K looks much broader and weaker than that in UD15K, which might have hindered its discovery in previous studies [26]. The strong intensity at small momentum transfer is due to the tails of the elastic peaks arising from the reflectivity of the surface at the specular angle.

To better visualize the charge order, we show the integral quasielastic intensities at 0 ± 0.04 eV for UD15K and OP33K in Figs. 2(a) and 2(b), respectively. We can directly observe the charge order with σ or π polarization at similar wave vector. We determined the full width at half maximum (FWHM) of charge order from σ polarization with more data points. By fitting the intensity with a power-law profile for the background and a Lorentzian function for the CDW peak, we determined the charge order vector to be ~0.26 rlu for UD15K and ~0.23 rlu for OP33K. The CDW peak intensity is weaker on top of a higher background in OP33K. For UD15K we

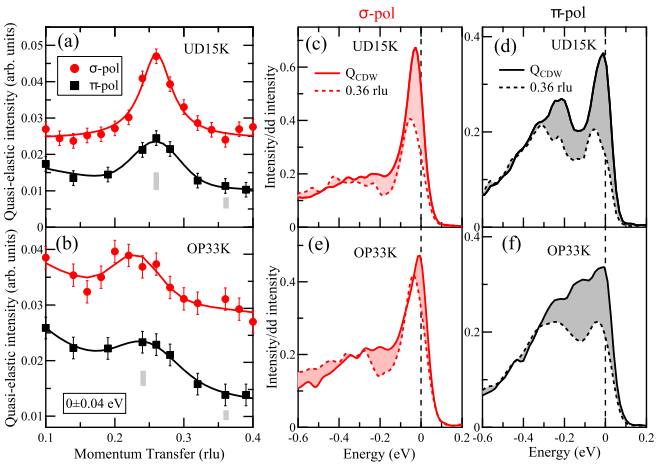

FIG. 2. Intensity at 0 ± 0.04 eV for the quasielastic signal along the (0,0)-(0.5,0) symmetry direction with π- or σ-polarized incident light at 20 K for UD15K (a) and OP33K (b). Solid lines are Lorentzian peak fits to the data with a power-law background. (c,d) Comparing the RIXS spectra of UD15K at Q_{CDW} and $Q_{\parallel} \simeq 0.36$ rlu as indicated by the gray bars in panel (a) with σ and π polarization, respectively. The differences between the two spectra are highlighted by the red (gray) shading for σ (π) polarization. (e,f) Similar to panels (c,d) but for OP33K.

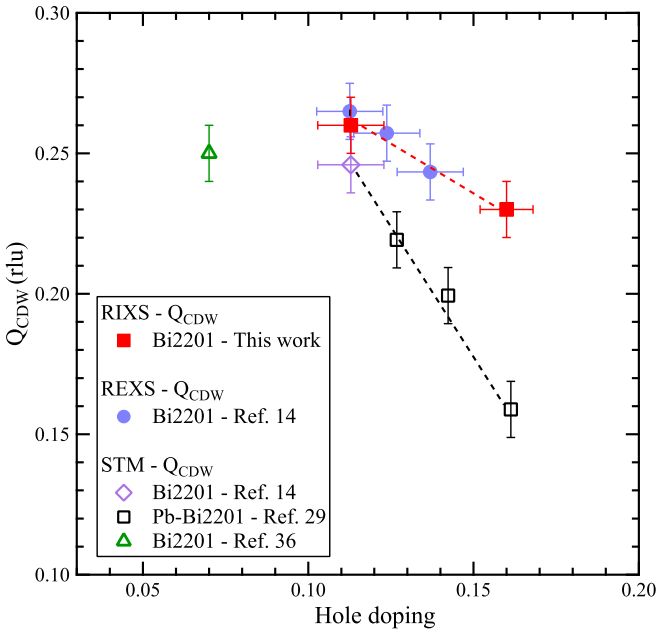

FIG. 3. Doping dependence of the charge order wave vector Q_{CDW}. Data from RXS [14] and STM [14,29,36] on Bi2201 are included. Bars represent errors due to uncertainty. Dashed lines are guides for the eye.

compare two spectra, one at $Q_{\mathrm{CDW}} \simeq 0.26$ rlu and the other at $Q_{\parallel} \simeq 0.36$ rlu, outside the CDW region, in Figs. 2(c) and 2(d) for σ and π polarization, respectively. Clearly, the elastic peak is much stronger at Q_{CDW}. In contrast, the quasielastic peak shifts to higher energy loss at $Q_{\parallel} \simeq 0.36$ rlu due to the phonon contributions. In π polarization there is also a prominent paramagnon feature, which disperses to higher energy with increasing momentum transfer as discussed previously [26]. For OP33K we observe similar trends in Figs. 2(e) and 2(f), but the spectral difference between the two momenta is smaller than that in UD15K.

In Fig. 3, we summarize the doping dependence of the charge order vector in Bi2201 from measurements by RIXS (our work), RXS [14], and STM [14,29,36]. The charge order vectors determined with RIXS follow the trend determined by RXS, while they are significantly larger than those obtained with STM measurements (see discussion below). When doping changes from $p \simeq 0.115$ to $p \simeq 0.16$, the FWHM of the CDW peak grows from 0.054 to 0.07 rlu, indicating a decreasing coherence length.

B. Momentum dependence

So far, we have focused on the charge order along the (0,0.5) or (0.5,0) direction. As already noted, the energy-integrated RXS measurement on Bi2201 gave no CDW signatures along the diagonal direction [30]. However, the checkerboardlike features observed by STM [29] might be induced by two kinds of charge modulation patterns, either along the Cu-O bond directions or along the nodal (diagonal) directions. Here we exploited the higher sensitivity of energy-resolved RIXS to ascertain this issue. As demonstrated above, UD15K shows a relatively strong CDW signal along the (0,0.5) or

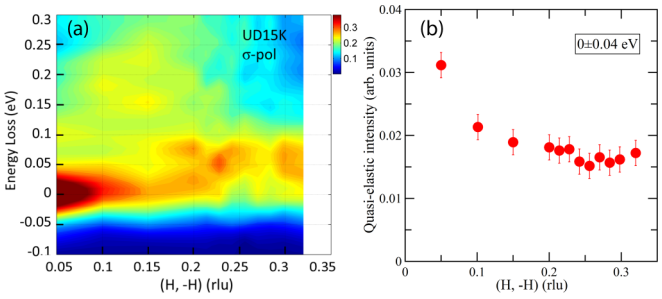

FIG. 4. (a) Energy/momentum intensity map of RIXS spectra along the (0,0)-(0.5,−0.5) symmetry direction taken with σ-polarized incident light at 20 K for UD15K. (b) Corresponding quasielastic intensity (integrated around 0 eV energy loss over ±0.04 eV range).

(0.5,0) direction with $Q_{CDW} \simeq 0.26$ rlu, which allows reaching the $(Q_{CDW}, -Q_{CDW})$ point; on the contrary in YBCO the hypothetical diagonal point at (0.31,0.31) is out of reach for Cu L_3 RIXS [10]. As shown in Fig. 4(a), along the (0.5,−0.5) direction, the energy/momentum intensity map of RIXS spectra shows no charge order signal at (0.26,−0.26) rlu around the quasi-elastic energy region, while there are clear phonon signals present at ∼55 meV. In comparison with the recent theoretical results [37] this signal is mostly due to the breathing phonon mode. Note that its intensity is far from being a smooth function of the momentum, indicating that the phonon may interact with other excitations. This study is very interesting in itself and requires a dedicated work beyond the purpose of the present paper. The quasielastic integrated intensity in Fig. 4(b) does not show any peak, in good agreement with prior results of RXS measurement on UD15K [30]. This confirms that the charge density modulates, unidirectionally, only along the Cu-O bonds. The orientation of CDW in cuprates has been discussed recently in a theoretical work based on the frustrated phase-separation model: along the diagonal the short-range residual repulsion is stronger than along Cu-O bonds so that the local effective attraction stabilizes the unidirectional CDW along the [1,0]/[0,1] direction instead of the [1,1] direction [38].

C. Temperature dependence

The temperature dependence of the charge order in UD15K has been reported in Ref. [14] with $T_{CDW} \simeq 240$ K ($\sim T^*$). In Fig. 5, we investigated the temperature dependence of the charge order across T_c and T^* for OP33K. From previous nuclear magnetic resonance (NMR) measurements on $Bi_2Sr_{2-x}La_xCuO_{6+\delta}$ [32], we know that the pseudogap temperature of OP33K is $T^* \simeq 160$ K. As shown in Figs. 5(a) and 5(b), the charge order can been seen clearly at 20 K and becomes sharper at $T_c \simeq 33$ K, with the width decreasing from 0.07 ± 0.01 rlu to 0.06 ± 0.01 rlu, as shown in Fig. 5(e). This behavior of the charge order is similar to that in YBCO [10], reflecting the competition between the CDW order and superconductivity. Above T_c the intensity of the charge order signal progressively decreases [10,14]. The charge order peak is still visible at 125 K, below T^*, but it disappears at 190 K, above T^*. Since the CDW onset temperature is not a thermodynamic phase boundary and given the statistical

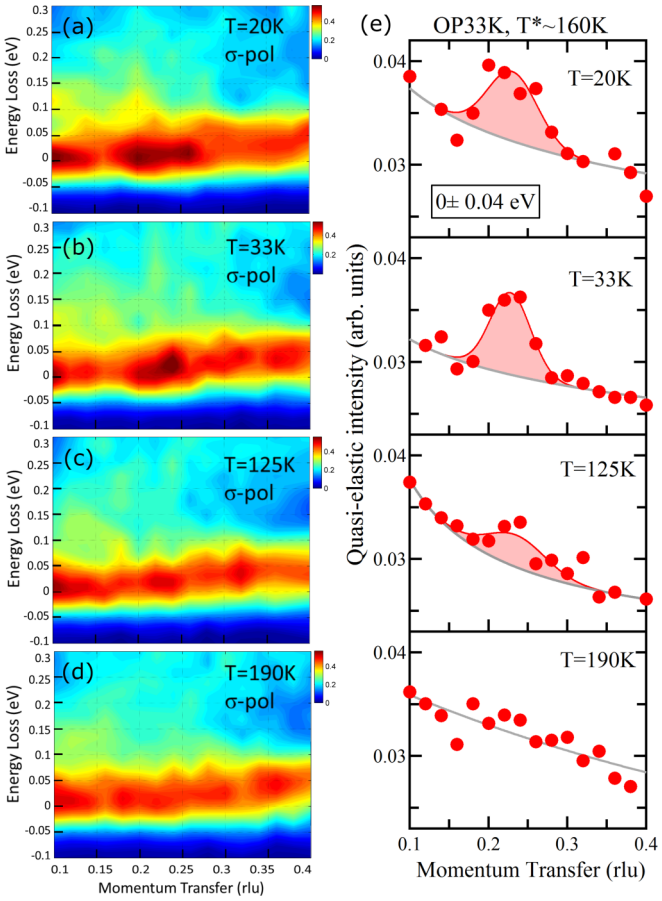

FIG. 5. Temperature dependence of charge order across $T_c \simeq 33$ K and $T^* \simeq 160$ K for OP33K. Energy/momentum intensity maps of RIXS spectra along the (0,0)-(0.5,0) symmetry direction measured at (a) 20 K, (b) 33 K, (c) 125 K, and (d) 190 K with σ polarization on OP33K. (e) Corresponding intensity at 0 ± 0.04 eV for the quasielastic signal. Solid lines are Lorentzian fits to the data with a power-law background. The areas after subtracting the background are highlighted by the red shading.

uncertainty in the high-temperature RIXS data, we are not able to determine whether the pseudogap formation precedes or coincides with the CDW order in OP33K.

D. *L* dependence

At zero magnetic field, the charge order peaks at half integer values of L in the out-of-plane direction both in YBCO [22,23] and LBCO [6–8]. Here, by exploiting the unique possibility available at ID32 of changing continuously the scattering angle in RIXS, we investigated the L dependence of the CDW in UD15K, to see whether or not there is an intensity maximum at half integer. In Figs. 6(a)–6(c) we show the energy/momentum intensity maps measured with three scattering angles ($2\theta = 140°, 123°, 110°$), corresponding to the charge order at (0.26, 0, 3), (0.26, 0, 2.75), and (0.26, 0, 2.5). We can see strong charge order signals in all three maps with similar quasielastic profiles as shown in Fig. 6(d). By fitting the data we obtained similar FWHMs (∼0.055 rlu) and correlation lengths (∼23 Å) for UD15K. We also performed a finer L scanning as shown in Fig. 7. For simplicity, instead of taking a full map at each L,

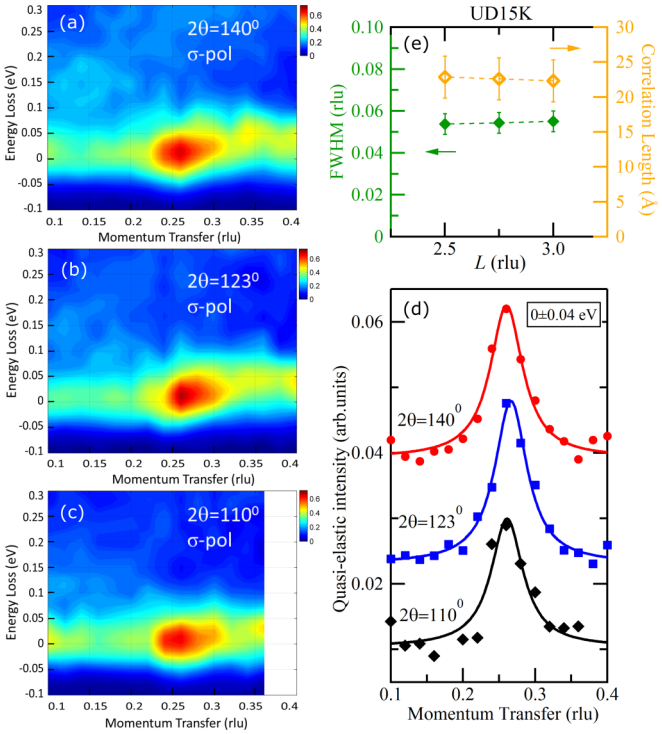

FIG. 6. Energy/momentum intensity maps of RIXS spectra along the (0,0)-(0.5,0) symmetry direction measured at (a) $2\theta = 140°$, (b) $2\theta = 123°$, and (c) $2\theta = 110°$ with σ polarization for UD15K at 20 K. (d) Integral intensity at 0 ± 0.04 eV for the quasielastic signal. Data are shifted vertically for clarity. Solid lines are Lorentzian fits to the data. (e) L dependence of the CDW peak FWHM, given in rlu (left) and corresponding correlation length (right) at 20 K. Dashed lines are guides to the eye.

we took a couple of RIXS spectra for each L, at Q_{CDW} and at $|Q_\phi|$, with $\phi = 20°$ in-plane rotation as defined in the inset and $|Q_\phi| = |Q_{\mathrm{CDW}}|$. The L values are ranging from 2.1 to 3.0 rlu. The difference between two spectra at the same L is marked by the green area, indicating the charge order intensity. In Fig. 7(b) we display the integral quasielastic intensities at Q_{CDW} and at Q_ϕ: neither of them display a maximum within error bar, not even at half integer L. In Fig. 7(c) we plot the intensity difference between the two momenta and again it shows no maximum at half integer nor at other values. Clearly the CDW intensity is flat across an entire Brillouin zone, demonstrating the complete absence of correlation along the c axis.

IV. DISCUSSION

A. Relation of charge order to antiferromagnetic and pseudogap state

We have found that charge order persists in Bi2201 up to optimal doping, consistently with LBCO [8], Bi2212 [16], and YBCO [18]. Our recent RIXS study on antiferromagnetic Bi2201 ($p = 0.03$) showed no charge order signals [39]. A recent STM experiment has reported a checkerboardlike charge order with wave vector $Q_{\mathrm{CDW}} \simeq 0.25$ rlu in lightly doped Bi2201 ($p = 0.07$, insulator) [36], demonstrating the charge order is the first electronic ordered state that emerges by doping the parent compound. The same work also confirmed the absence of a checkerboardlike pattern at very low doping, $p = 0.03$ [36], in agreement with our RIXS results. The evidence of charge order in the AF insulating regime is incompatible with the "Fermi arc nesting" scenario which correlates the Q_{CDW} to the distance between the Fermi-arc tips [14], because in single layer Bi2201 the Fermi surface is fully gapped below the antiferromagnetic critical point $p = 0.1$ [40]. Note that it has been proposed that the emergence of the checkerboard structure is a consequence of the proximity to an antiferromagnetic quantum critical point [41,42].

In the SC regime above the critical doping $p = 0.1$, the charge order vector and its correlation length decrease with doping. As summarized in Fig. 3, the CDW order in Bi2201 has been experimentally detected for $p_{c_1} \leqslant p \leqslant p_{c_2}$ with $p_{c_1} \backsimeq 0.07$ and $p_{c_2} \backsimeq 0.16$. We notice that there is a non-negligible discrepancy between charge order vectors determined from STM and RXS. The latter gives in general larger CDW vectors. The difference increases with doping and reaches 35% in the optimal doping, which is out of the error tolerance. This may reflect the bulk (x-ray scattering) and surface (STM) dichotomy of the charge order, like the observation of the bulk-surface dichotomy of the superstructure modulations in the diagonal direction [43]. It is known that the carrier concentration is different at the surface and in the bulk and that the difference grows with doping. The CDW order arising from the charge modulations can reflect this dichotomy: indeed at low doping $p \simeq 0.11$ the Q_{CDW} vectors are similar between RXS and STM results, while they separate into two trends and depart further with doping. A recent STM work, by utilizing the phase-resolved electronic structure visualization, has revealed a surprising doping independent locking of the local CDW wave vector at 0.25 rlu throughout the underdoped phase diagram of (bilayer) Bi2212 [44]. While the generality of this lattice-commensurability CDW in other cuprates and the supposed correlation with x-ray scattering results through phase slips between different short-ranged correlated domains remain to be explored, at least the conventional CDW amplitudes probed by x-ray and STM look different.

If compared to other cuprates, the charge order in Bi2201 is rather short ranged, with a real-space correlation length between 17 and 23 Å, similar to ~24 Å in Bi2212 [16], but shorter than 20–70 Å in YBCO [18] and 150–250 Å in LBCO [7,8]. Probably lager disorder (e.g., chemical inhomogeneity) plays a bigger role in Bi2201 and Bi2212 [45]. The charge order has not been observed in the overdoped regime of cuprates, according to the few attempts reported in literature [10,18]. For Bi2201 the pseudogap state extends to the heavily overdoped regime, which is well defined by the NMR measurements [32] [Fig. 1(a)]. Therefore the end point of pseudogap state does not coincide with the end point of charge order in Bi2201. Also in YBCO the high magnetic field Hall coefficient measurements showed that the Fermi surface reconstruction by charge order ended at the optimal doping $p = 0.16$ [46], which is distinctly lower than the pseudogap critical point $p = 0.19$ [47]. As Keimer *et al.* [21] have already pointed out, the pseudogap is characterized by several competing ordering tendencies and it would not be surprising that the critical points between the pseudogap and the charge order do not coincide, although the opposite is not excluded

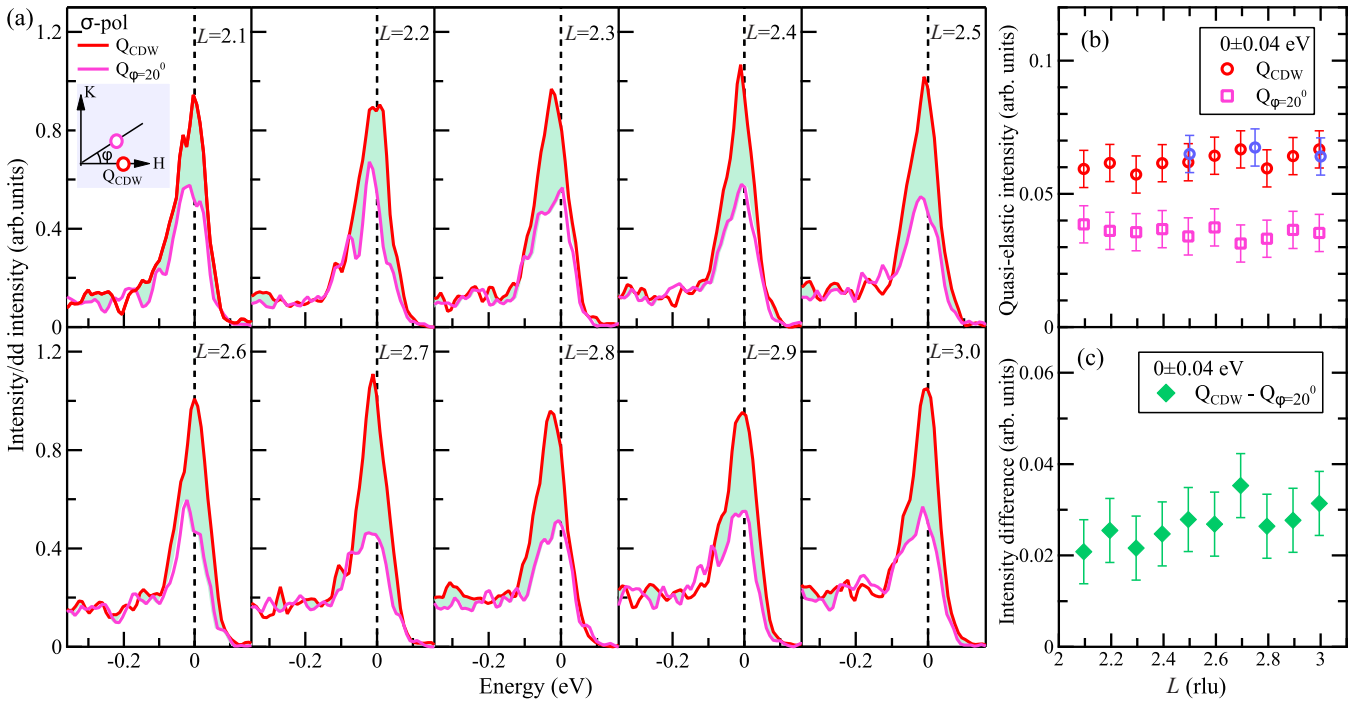

FIG. 7. (a) Comparison of RIXS spectra of UD15K at Q_{CDW} and at Q_{ϕ} with $\phi = 20^{\circ}$ as defined in the inset, measured with σ polarization from $L = 2.1$ to 3.0 rlu. Data were collected at 20 K. The differences between two spectra at the same L are highlighted by the green shading. A self-absorption correction has been applied to the intensities. (b) L dependence of the quasielastic intensity within 0 ± 0.04 eV at Q_{CDW} (hollow red circles) and at $Q_{\phi=20^{\circ}}$ (hollow magenta square). Three data points from Fig. 6 are also included (hollow blue circles). (c) The intensity differences between Q_{CDW} and $Q_{\phi=20^{\circ}}$. The error bars represent the uncertainty in determining the spectral weight.

too. Moreover, which termination point (as determined by Fermi surface reconstruction [46,48], symmetry breaking [49], divergent effective mass [50], etc.) actually relates to the QCP is hotly debated, and there is a need for further experimental and theoretical investigations.

B. Correlation of charge order along the *c* direction

Besides the in-plane components, x-ray studies of the charge order in YBCO and LBCO have reported an additional correlation along the c direction [6–8,12,22,23]. This depends on the relative (from plane to plane) phase of the CDW modulations along the c direction. In zero magnetic field, x-ray diffraction of the ionic displacements in YBCO [31] revealed a weak antiphase correlation in neighboring bilayers, which results in the CDW peaking at half-integral values of L. This finite c-axis coherence of the CDW is rather short ranged, with a length of $\backsim 9 \pm 3$ Å(i.e., approximately the distance between two adjacent bilayers) [31]. By applying high magnetic fields (typically $B > 15$ T), the c direction behavior of the CDW evolves differently along the a and b directions: the correlation simply becomes stronger in the a direction while a new peak appears at $L = 1$ along the b direction with increasing correlation length $\sim 4c$ [23]. This means the CDWs propagating along the a axis keep antiphase correlation between neighboring bilayers while those propagating along the b axis lock their phase with neighboring bilayers. In LBCO the charge stipe order also exhibits broad maxima at half-integer L, indicative of a twofold periodicity along the c axis [6–8]. The reason is that in adjacent planes within one unit cell the stripes align in orthogonal directions arising from the tilting pattern of the CuO_6 octahedra. In addition, the charge order is offset by $2a$ between successive unit cells, presumably to minimize Coulomb repulsion, resulting in an antiphase relationship between next-nearest-neighbor CuO_2 planes [6–8]. This out-of-plane correlation is very short ranged $\sim$5–10 Å ($<c$) and can be enhanced by a magnetic field [51].

On the other hand, our c direction study of CDW in Bi2201 does not show any peak, indicating there is no phase correlation of CDW along the c direction. The underlying reason can be the following: the distance between the adjacent Cu-O planes in Bi2201 is $\sim$12.2 Å within one unit cell, and neighboring planes are offset by (0.5,0.5): CDW correlation is discouraged both by distance and crystalline mismatch, resulting in random phases along the c direction. There is no high magnetic field measurement on Bi2201 yet, but the 2D CDW is to be expected, since the coupling between the two CuO_2 planes within one unit cell is rather weak, let alone the coupling between two unit cells. For double-layer Bi2212, we infer that the charge order also has no phase correlation along the c direction, because the distance between two bilayers is $\sim$12.3 Å, much larger than in YBCO ($\sim$8.5 Å), which maybe also discouraged by the (0.5,0.5) offset.

V. CONCLUSIONS

We have directly observed a bulk, incommensurate charge order in UD15K and OP33K, demonstrating that the short-range charge density modulations persist up to optimal doping in Bi2201. Both the CDW intensity and the correlation length

decrease with doping. In addition, the CDW vector decreases with doping, showing a bulk/surface dichotomy from RXS and STM measurements. The doping range of charge order in Bi2201, $p_{c_1} \leqslant p \leqslant p_{c_2}$ with $p_{c_1} \backsimeq 0.07$ and $p_{c_2} \backsimeq 0.16$, suggests the critical points of charge order are different from those of the AF, SC, and pseudogap regions. Thus, charge order appears to be a separate phenomenon that coexists with the AF, SC, and pseudogap regions. Temperature measurements have demonstrated that it competes with superconductivity and the signal disappears across T^* due to fluctuations. Whether and how it relates to QCP for the mechanism of high-T_c superconductivity requires future experimental and theoretical research. Furthermore, we confirmed there is no charge order along the diagonal direction, suggesting the CDW propagates only along the Cu-O bond direction. This fact is also compatible with the observed L independence of CDW, indicating there is no phase correlations along the c direction at variance with YBCO and LBCO and hinting at a perfectly two-dimensional charge ordering in single layer Bi2201.

ACKNOWLEDGMENTS

The experimental data were collected at the beam line ID32 of the European Synchrotron (ESRF) in Grenoble (France) using the ERIXS spectrometer designed jointly by the ESRF and the Politecnico di Milano. This work was supported by MIUR Italian Ministry for Research through project PIK Polarix. X.J.Z. acknowledges the support from the NSFC (Grant No. 11334010), the National Key Research and Development Program of China (Grant No. 2016YFA0300300), and the Strategic Priority Research Program (B) of the Chinese Academy of Sciences (Grant No. XDB07020300). We thank Marc-Henri Julien and Eric Eyraud for their help with the characterization of some samples. We gratefully acknowledge the support of all the staff of the ID32 beam line of the ESRF, in particular, Flora Yakhou-Harris, Andrea Fondacaro, and Andrea Amorese.

[1] J. G. Bednorz and K. A. Müller, Z. Phys. B **64**, 189 (1986).
[2] P. A. Lee, N. Nagaosa, and X. G. Wen, Rev. Mod. Phys. **78**, 17 (2006).
[3] T. Timusk and B. Statt, Rep. Prog. Phys. **62**, 61 (1999).
[4] J. M. Tranquada, B. J. Sternlieb, J. D. Axe, Y. Nakamura, and S. Uchida, Nature (London) **375**, 561 (1995).
[5] M. Fujita, H. Goka, K. Yamada, and M. Matsuda, Phys. Rev. Lett. **88**, 167008 (2002).
[6] H. Kimura, H. Goka, M. Fujita, Y. Noda, K. Yamada, and N. Ikeda, Phys. Rev. B **67**, 140503 (2003).
[7] P. Abbamonte, A. Rusydi, S. Smadici, G. D. Gu, G. A. Sawatzky, and D. L. Feng, Nat. Phys. **1**, 155 (2005).
[8] M. Hücker, M. v. Zimmermann, G. D. Gu, Z. J. Xu, J. S. Wen, G. Xu, H. J. Kang, A. Zheludev, and J. M. Tranquada, Phys. Rev. B **83**, 104506 (2011).
[9] T. Wu, H. Mayaffre, S. Krämer, M. Horvatić, C. Berthier, W. N. Hardy, R. X. Liang, D. A. Bonn, and M.-H. Julien, Nature (London) **477**, 191 (2011).
[10] G. Ghiringhelli, M. Le Tacon, M. Minola, S. Blanco-Canosa, C. Mazzoli, N. B. Brookes, G. M. De Luca, A. Fraño, D. G. Hawthorn, F. He, T. Loew, M. M. Sala, D. C. Peets, M. Salluzzo, E. Schierle, R. Sutarto, G. A. Sawatzky, E. Weschke, B. Keimer, and L. Braicovich, Science **337**, 821 (2012).
[11] A. J. Achkar, R. Sutarto, X. Mao, F. He, A. Fraño, S. Blanco-Canosa, M. Le Tacon, G. Ghiringhelli, L. Braicovich, M. Minola, M. Moretti Sala, C. Mazzoli, R. Liang, D. A. Bonn, W. N. Hardy, B. Keimer, G. A. Sawatzky, and D. G. Hawthorn, Phys. Rev. Lett. **109**, 167001 (2012).
[12] J. Chang, E. Blackburn, A. T. Holmes, N. B. Christensen, J. Larsen, J. Mesot, R. Liang, D. A. Bonn, W. N. Hardy, A. Watenphul, M. v. Zimmermann, E. M. Forgan, and S. M. Hayden, Nat. Phys. **8**, 871 (2012).
[13] E. Blackburn, J. Chang, M. Hücker, A. T. Holmes, N. B. Christensen, R. Liang, D. A. Bonn, W. N. Hardy, U. Rütt, O. Gutowski, M. v. Zimmermann, E. M. Forgan, and S. M. Hayden, Phys. Rev. Lett. **110**, 137004 (2013).
[14] R. Comin, A. Fraño, M. M. Yee, Y. Yoshida, H. Eisaki, E. Schierle, E. Weschke, R. Sutarto, F. He, A. Soumyanarayanan, Y. He, M. Le Tacon, I. Elfimov, J. E. Hoffman, G. Sawatzky, B. Keimer, and A. Damascelli, Science **343**, 390 (2014).
[15] E. H. da Silva Neto, P. Aynajian, A. Fraño, R. Comin, E. Schierle, E. Weschke, A. Gyenis, J. S. Wen, J. Schneeloch, Z. J. Xu, S. Ono, G. D. Gu, M. Le Tacon, and Ali Yazdani, Science **343**, 393 (2014).
[16] M. Hashimoto, G. Ghiringhelli, W.-S. Lee, G. Dellea, A. Amorese, C. Mazzoli, K. Kummer, N. B. Brookes, B. Moritz, Y. Yoshida, H. Eisaki, Z. Hussain, T. P. Devereaux, Z.-X. Shen, and L. Braicovich, Phys. Rev. B **89**, 220511(R) (2014).
[17] W. Tabis, Y. Li, M. Le Tacon, L. Braicovich, A. Kreyssig, M. Minola, G. Dellea, E. Weschke, M. J. Veit, M. Ramazanoglu, A. I. Goldman, T. Schmitt, G. Ghiringhelli, N. Barišić, M. K. Chan, C. J. Dorow, G. Yu, X. Zhao, B. Keimer, and M. Greven, Nat. Commun. **5**, 5875 (2014).
[18] S. Blanco-Canosa, A. Fraño, E. Schierle, J. Porras, T. Loew, M. Minola, M. Bluschke, E. Weschke, B. Keimer, and M. Le Tacon, Phys. Rev. B **90**, 054513 (2014).
[19] E. H. da Silva Neto, R. Comin, F. He, R. Sutarto, Y. Jiang, R. L. Greene, G. A. Sawatzky, and A. Damascelli, Science **347**, 1335 (2015).
[20] E. H. da Silva Neto, B. Q. Yu, M. Minola, R. Sutarto, E. Schierle, F. Boschini, M. Zonno, M. Bluschke, J. Higgins, Y. M. Li, G. C. Yu, E. Weschke, F. Z. He, M. Le Tacon, R. L. Greene, M. Greven, G. A. Sawatzky, B. Keimer, and A. Damascelli, Sci. Adv. **2**, 1600782 (2016).
[21] B. Keimer, S. A. Kivelson, M. R. Norman, S. Uchida, and J. Zaanen, Nature (London) **518**, 179 (2015).
[22] S. Gerber, H. Jang, H. Nojiri, S. Matsuzawa, H. Yasumura, D. A. Bonn, R. Liang, W. N. Hardy, Z. Islam, A. Mehta, S. Song, M. Sikorski, D. Stefanescu, Y. Feng, S. A. Kivelson, T. P. Devereaux, Z.-X. Shen, C.-C. Kao, W.-S. Lee, D. Zhu, and J.-S. Lee, Science **350**, 949 (2015).
[23] J. Chang, E. Blackburn, O. Ivashko, A. T. Holmes, N. B. Christensen, M. Hücker, R. Liang, D. A. Bonn, W. N. Hardy,

U. Rütt, M. v. Zimmermann, E. M. Forgan, and S. M. Hayden, Nat. Commun. **7**, 11494 (2016).
[24] N. Doiron-Leyraud, C. Proust, D. LeBoeuf, J. Levallois, J. B. Bonnemaison, R. X. Liang, D. A. Bonn, W. N. Hardy, and L. Taillefer, Nature (London) **447**, 565 (2007).
[25] S. E. Sebastian, N. Harrison, E. Palm, T. P. Murphy, C. H. Mielke, R. X. Liang, D. A. Bonn, W. N. Hardy, and G. G. Lonzarich, Nature (London) **454**, 200 (2008).
[26] Y. Y. Peng, M. Hashimoto, M. M. Sala, A. Amorese, N. B. Brookes, G. Dellea, W.-S. Lee, M. Minola, T. Schmitt, Y. Yoshida, K.-J. Zhou, H. Eisaki, T. P. Devereaux, Z.-X. Shen, L. Braicovich, and G. Ghiringhelli, Phys. Rev. B **92**, 064517 (2015).
[27] M. Hashimoto, R.-H. He, K. Tanaka, J.-P. Testaud, W. Meevasana, R. G. Moore, D. H. Lu, H. Yao, Y. Yoshida, H. Eisaki, T. P. Devereaux, Z. Hussain, and Z.-X. Shen, Nat. Phys. **6**, 414 (2010).
[28] R.-H. He *et al.*, Science **331**, 1579 (2011).
[29] W. D. Wise, M. C. Boyer, K. Chatterjee, T. Kondo, T. Takeuchi, H. Ikuta, Y. Wang, and E. W. Hudson, Nat. Phys. **4**, 696 (2008).
[30] R. Comin, R. Sutarto, F. He, E. H. da Silva Neto, L. Chauviere, A. Fraño, R. Liang, W. N. Hardy, D. A. Bonn, Y. Yoshida, H. Eisaki, A. J. Achkar, D. G. Hawthorn, B. Keimer, G. A. Sawatzky, and A. Damascelli, Nat. Mater. **14**, 796 (2015).
[31] E. M. Forgan, E. Blackburn, A. T. Holmes, A. K. R. Briffa, J. Chang, L. Bouchenoire, S. D. Brown, R. X. Liang, D. Bonn, W. N. Hardy, N. B. Christensen, M.v. Zimmermann, M. Hücker and S. M. Hayden, Nat. Commun. **6**, 10064 (2015).
[32] S. J. Kawasaki, C. T. Lin, P. L. Kuhns, A. P. Reyes, and G.-Q. Zheng, Phys. Rev. Lett. **105**, 137002 (2010).
[33] J. Q. Meng, G. D. Liu, W. T. Zhang, L. Zhao, H. Y. Liu, W. Lu, X. L. Dong, and X. J. Zhou, Supercond. Sci. Technol. **22**, 045010 (2009).
[34] Z. Chen, Y. Y. Peng, Z. Wang, Y. J. Song, J. Q. Meng, X. J. Zhou, and J. Q. Li, Supercond. Sci. Technol. **26**, 055010 (2013).
[35] L. Braicovich, M. Moretti Sala, L. J. P. Ament, V. Bisogni, M. Minola, G. Balestrino, D. Di Castro, G. M. De Luca, M. Salluzzo, G. Ghiringhelli, and J. van den Brink, Phys. Rev. B **81**, 174533 (2010).
[36] P. Cai, W. Ruan, Y. Y. Peng, C. Ye, X. T. Li, Z. Q. Hao, X. J. Zhou, D.-H. Lee, and Y. Y. Wang, Nat. Phys. **12**, 1047 (2016).
[37] T. P. Devereaux, A. M. Shvaika, K. Wu, K. Wohlfeld, C. J. Jia, Y. Wang, B. Moritz, L. Chaix, W.-S. Lee, Z.-X. Shen, G. Ghiringhelli, and L. Braicovich, Phys. Rev. X **6**, 041019 (2016).
[38] S. Caprara, C. Di Castro, G. Seibold, and M. Grilli, arXiv:1604.07852v2.
[39] Y. Y. Peng, G. Dellea, M. Minola, M. Conni, A. Amorese, D. Di Castro, G. M. De Luca, K. Kummer, M. Salluzzo, X. Sun, X. J. Zhou, G. Balestrino, M. Le Tacon, B. Keimer, L. Braicovich, N. B. Brookes, and G. Ghiringhelli, arXiv:1609.05405.
[40] Y. Y. Peng, J. Q. Meng, D. X. Mou, J. F. He, L. Zhao, Y. Wu, G. D. Liu, X. L. Dong, S. L. He, J. Zhang, X. Y. Wang, Q. J. Peng, Z. M. Wang, S. J. Zhang, F. Yang, C. T. Chen, Z. Y. Xu, T. K. Lee, and X. J. Zhou, Nat. Commun. **4**, 2459 (2013).
[41] K. B. Efetov, H. Meier, and C. Pépin, Nat. Phys. **9**, 442 (2013).
[42] H. Meier, C. Pépin, M. Einenkel, and K. B. Efetov, Phys. Rev. B **89**, 195115 (2014).
[43] J. A. Rosen *et al.*, Nat Commun. **4**, 1977 (2013).
[44] A. Mesaros, K. Fujita, S. D. Edkins, M. H. Hamidian, H. Eisaki, S. Uchida, J. C. Séamus Davis, M. J. Lawler, and Eun-Ah Kim, Proc. Natl. Acad. Sci. USA **113**, 12661 (2016).
[45] H. Eisaki, N. Kaneko, D. L. Feng, A. Damascelli, P. K. Mang, K. M. Shen, Z.-X. Shen, and M. Greven, Phys. Rev. B **69**, 064512 (2004).
[46] S. Badoux, W. Tabis, F. Laliberté, G. Grissonnanche, B. Vignolle, D. Vignolles, J. Béard, D. A. Bonn, W. N. Hardy, R. Liang, N. Doiron-Leyraud, L. Taillefer, and C. Proust, Nature (London) **531**, 210 (2016).
[47] J. L. Tallon and J. W. Loram, Phys. C **349**, 53 (2001).
[48] Y. He, Y. Yin, M. Zech, A. Soumyanarayanan, M. M. Yee, T. Williams, M. C. Boyer, K. Chatterjee, W. D. Wise, I. Zeljkovic, T. Kondo, T. Takeuchi, H. Ikuta, P. Mistark, R. S. Markiewicz, A. Bansil, S. Sachdev, E. W. Hudson, and J. E. Hoffman, Science **344**, 608 (2014).
[49] K. Fujita, C. K. Kim, I. Lee, J. Lee, M. H. Hamidian, I. A. Firmo, S. Mukhopadhyay, H. Eisaki, S. Uchida, M. J. Lawler, E.-A. Kim, and J. C. Davis, Science **344**, 612 (2014).
[50] B. J. Ramshaw, S. E. Sebastian, R. D. McDonald, J. Day, B. S. Tan, Z. Zhu, J. B. Betts, R. Liang, D. A. Bonn, W. N. Hardy, and N. Harrison, Science **348**, 317 (2015).
[51] M. Hücker, M. v. Zimmermann, Z. J. Xu, J. S. Wen, G. D. Gu, and J. M. Tranquada, Phys. Rev. B **87**, 014501 (2013).